Inorganic Chemistry

Article

pubs.acs.org/IC

C−H Bond Oxidation Catalyzed by an Imine-Based Iron Complex: A Mechanistic Insight

Giorgio Olivo,[§,¶] Martina Nardi,[§] Diego Vìdal,[¶] Alessia Barbieri,[§] Andrea Lapi,[§,‡] Laura Gómez,[¶,⊥] Osvaldo Lanzalunga,[§,‡] Miquel Costas,*[,¶] and Stefano Di Stefano*[,§,‡]

[§]Dipartimento di Chimica, Università degli Studi di Roma "La Sapienza" and Istituto CNR di Metodologie Chimiche (IMC−CNR), Sezione Meccanismi di Reazione, c/o Dipartimento di Chimica, Università degli Studi di Roma "La Sapienza", P.le A. Moro 5, I-00185 Rome, Italy

[¶]Institut de Química Computacional i Catàlisi (IQCC) and Departament de Química, Universitat de Girona, Campus de Montilivi, 17071 Girona, Spain

[‡]Consortium of Chemical Catalysis and Reactivity, CIRCC Interuniversity, Via Celso Ulpiani 27, 70126 Bari, Italy

[⊥]Serveis Tècnics de Recerca (STR), Universitat de Girona, Parc Científic i Tecnològic, E-17003 Girona, Spain

Supporting Information

ABSTRACT: A family of imine-based nonheme iron(II) complexes $(\mathbf{LX})_2Fe(OTf)_2$ has been prepared, characterized, and employed as C−H oxidation catalysts. Ligands **LX** (**X** = **1**, **2**, **3**, and **4**) stand for tridentate imine ligands resulting from spontaneous condensation of 2-pycolyl-amine and 4-substituted-2-picolyl aldehydes. Fast and quantitative formation of the complex occurs just upon mixing aldehyde, amine, and $Fe(OTf)_2$ in a 2:2:1 ratio in acetonitrile solution. The solid-state structures of $(\mathbf{L1})_2Fe(OTf)(ClO_4)$ and $(\mathbf{L3})_2Fe(OTf)_2$ are reported, showing a low-spin octahedral iron center, with the ligands arranged in a meridional fashion. ^{1}H NMR analyses indicate that the solid-state structure and spin state is retained in solution. These analyses also show the presence of an amine-imine tautomeric equilibrium. $(\mathbf{LX})_2Fe(OTf)_2$ efficiently catalyze the oxidation of alkyl C−H bonds employing H_2O_2 as a terminal oxidant. Manipulation of the electronic properties of the imine ligand has only a minor impact on efficiency and selectivity of the oxidative process. A mechanistic study is presented, providing evidence that C−H oxidations are metal-based. Reactions occur with stereoretention at the hydroxylated carbon and selectively at tertiary over secondary C−H bonds. Isotopic labeling analyses show that H_2O_2 is the dominant origin of the oxygen atoms inserted in the oxygenated product. Experimental evidence is provided that reactions involve initial oxidation of the complexes to the ferric state, and it is proposed that a ligand arm dissociates to enable hydrogen peroxide binding and activation. Selectivity patterns and isotopic labeling studies strongly suggest that activation of hydrogen peroxide occurs by heterolytic O−O cleavage, without the assistance of a *cis*-binding water or alkyl carboxylic acid. The sum of these observations provides sound evidence that controlled activation of H_2O_2 at $(\mathbf{LX})_2Fe(OTf)_2$ differs from that occurring in biomimetic iron catalysts described to date.

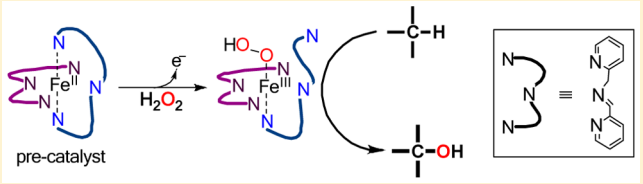

INTRODUCTION

During the past decade, nonheme iron(II) complexes of poliazotate ligands have shown a great potential as catalysts for effective C−H bond oxidations with high levels of regio- and chemo-selectivity.[1] These complexes can oxidize nonactivated C−H bonds in aliphatic compounds with predictable selectivity patterns, using inexpensive and waste-free hydrogen peroxide as the terminal oxidant. The selectivity is retained, even in challenging C−H oxidations of complex molecular scaffolds.[2] Much effort has been devoted to the comprehension of the catalytic mechanisms and to the identification of the intermediates competent for such oxidative transformations. Besides the importance in chemical synthesis, these mechanisms and the species implicated therein receive interest because of their relevance to understand the paths of oxidations performed at iron oxygenases.[1a,3] It is generally accepted that the initial Fe^{II} complex reacts with excess H_2O_2 to form an Fe(III)−OOH intermediate[3a,4] (or an Fe^{III}-acylperoxo species when a carboxylic acid is present in the reaction mixture[5]). This peroxide intermediate subsequently undergoes O−O bond cleavage with the formation of either an Fe^{IV}=O by homolysis or a formal Fe^{V}=O species by heterolysis, the latter assisted by a coordinated water or carboxylic acid molecule.[3a,4,5] Two *cis* labile coordination sites on the Fe ion are necessary to enable heterolytic O−O cleavage to occur in most cases, while related complexes with pentadentate ligands engage in homolytic O−O lysis.[4b−d] O−O bond homolysis usually leads to radical chain oxidation mechanisms,[4c,d,f,g] with the exception of specific cases due to reaction conditions,[4h] while O−O heterolysis is thought to generate selective, metal-based oxidants.[3a,d,6,7] Computational and some experimental evidence indicate that the actual

Received: April 2, 2015

DOI: 10.1021/acs.inorgchem.5b01500
Inorg. Chem. XXXX, XXX, XXX−XXX

Scheme 1

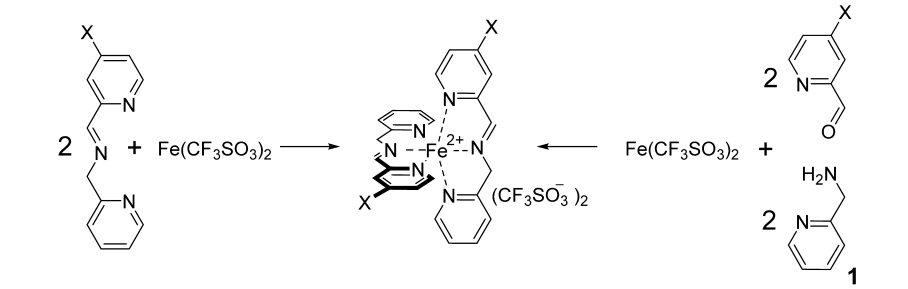

X=H $(\mathbf{L1})_2Fe(OTf)_2$
X=OCH_3 $(\mathbf{L2})_2Fe(OTf)_2$
X=CH_3 $(\mathbf{L3})_2Fe(OTf)_2$
X=NO_2 $(\mathbf{L4})_2Fe(OTf)_2$

oxidant that forms after O−O cleavage is a $Fe^{V}(O)(OH)$ species in the water-assisted mechanism,[3b,4b,6,7] and a $Fe^{V}(O)(OAc)$ or a $Fe^{IV}(O)(^{\bullet}OAc)$ complex when acetic acid is assisting the process.[5] A single example has been described by Hitomi that departs from this situation, where the strong *trans* effect exerted by an anionic amide ligand facilitates heterolytic O−O cleavage in a ferric complex with a pentadentate ligand.[2e,8] However, further studies are still needed in order to confirm this mechanistic scenario and to identify and fully characterize the real oxidizing species.

The selectivity in the oxidations catalyzed by nonheme iron complexes is dictated primarily by stereoelectronic effects (the most electron-rich and sterically accessible C−H bonds in the substrate are the most easily oxidized).[2a,c,9] In addition, structural features of the catalyst might also play a key role in this respect. Increase of the catalyst steric hindrance and consequent decrease of accessibility to the active iron-oxo moiety can even overcome the innate reactivity of C−H bonds in favor of the least sterically encumbered secondary or tertiary ones.[2f−h] However, these bulky catalysts usually require rather elaborate ligands, which limit their use.

With the main objective of simplifying ligand structures, some of us have started to explore the activity of imine-based iron complexes, which are far less studied than the amine-based ones, despite the much greater ease of preparation of imines,[10] in comparison with amines. Former imine-based complexes have been explored in the oxidation of simple cycloalkanes, showing reactivity patterns characteristic of free-diffusing radical reactions, and moderate TONs.[2j,11,12] Nevertheless, we recently communicated that a simple imine-based nonheme iron(II) complex[13] (complex $(\mathbf{L1})_2Fe(OTf)_2$ depicted in Scheme 1) catalyzes alkane hydroxylation with efficiencies (TONs in the range of 15−48) comparable to those obtained with much more sophisticated amine-based catalysts.[2,14] Complex $(\mathbf{L1})_2Fe(OTf)_2$ can be readily prepared just by simply mixing commercially available, nonexpensive reagents (iron salt, aldehyde, and amine) in the reaction vessel, with no prior synthesis and isolation required. Herein, we report the solid-state and solution-state characterization of $(\mathbf{L1})_2Fe(OTf)_2$, and a detailed mechanistic investigation of alkane oxidation mediated by $(\mathbf{L1})_2Fe(OTf)_2$. Substrate probe oxidations are carried out in order to distinguish between a mechanism involving free diffusing radicals and a metal-based oxidation. The origin of the O atom incorporated into hydroxylated products is ascertained by means of isotopic labeling experiments. Further insight into the oxidation mechanism is collected by monitoring catalyst $(\mathbf{L1})_2Fe(OTf)_2$ evolution throughout the reaction. Finally, a study of substituent effects of the imine ligands on the corresponding complexes catalytic activity and selectivity was conducted. The sum of the experimental observations shows that $(\mathbf{L1})_2Fe(OTf)_2$ has the potential to be the prototype of a novel class of catalysts that activates H_2O_2 via a mechanism that does not involve two *cis*-labile sites, and carries out site-selective hydroxylation of alkane C−H bonds with stereoretention.

RESULTS AND DISCUSSION

Characterization of complexes $(\mathbf{L1}-\mathbf{L4})_2Fe(OTf)_2$. We recently reported that rapid and quantitative assembly of complex $(\mathbf{L1})_2Fe(OTf)_2$ occurs in acetonitrile solution upon mixing 2-picolyl aldehyde, 2-picolyl amine, and $Fe(OTf)_2$ in a 2:2:1 ratio, as ascertained by a UV−vis spectrophotometric titration.[13] The stoichiometry of the complex was further confirmed after isolating and characterizing the complex in crystalline form (see the Experimental Section). The solid-state structure of double salt $(\mathbf{L1})_2Fe(OTf)(ClO_4)$, obtained via the crystallization of $(\mathbf{L1})_2Fe(OTf)_2$ in the presence of $NaClO_4$, is reported in Figure 1 as an ORTEP diagram. The crystal data

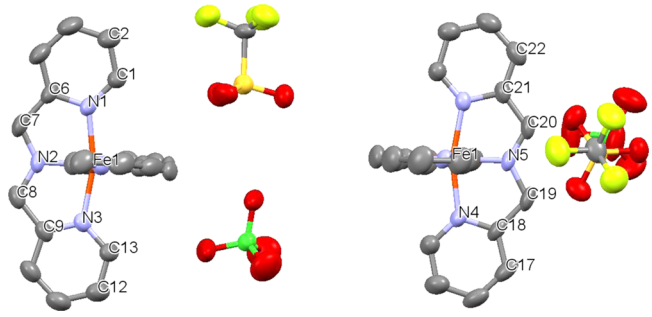

Figure 1. ORTEP diagram corresponding to the X-ray structure of complex $(\mathbf{L1})_2Fe(OTf)(ClO_4)$. Right image is obtained by 90° rotation around *x*-axis of the left one. Crystal data and a list of selected bond lengths and angles are reported in Tables SI 1 and SI 2 in the Supporting Information. Hydrogen atoms are omitted for clarity.

DOI: 10.1021/acs.inorgchem.5b01500
Inorg. Chem. XXXX, XXX, XXX−XXX

and a list of selected bond lengths and angles of $(\mathbf{L1})_2$Fe(OTf)(ClO_4) are reported in the Supporting Information (Tables SI 1 and SI 2, respectively). This complex crystallizes in the monoclinic crystal system, and it adopts a slightly distorted octahedral geometry. The two ligand units chelate the metal in a meridional fashion, occupying the first Fe coordination sphere. The two iminic N atoms are *trans* to each other. Counterions lie in the second coordination sphere and show close contact interactions with aminic C_{19} and iminic C_{20} carbons, as well as with the C_1-C_2 and $C_{12}-C_{13}$ pyridine carbons of the opposite ligand unit. The short Fe−N bond lengths (1.88−1.98 Å) are diagnostic for a low-spin ferrous center,[4c,15] which has a smaller ionic radius than the high spin one. Fe−N imine distances are slightly shorter (~0.1 Å) than the Fe−N pyridine distances. The low-spin nature of complex $(\mathbf{L1})_2$Fe$(OTf)_2$ is retained in CD_3CN solution, as shown by the compact spectral window of its ^{1}H NMR spectrum (1−10.5 ppm), characteristic of diamagnetic species (see Figure SI 1 in the Supporting Information). Also, temperature does not affect the structure of complex $(\mathbf{L1})_2$Fe$(OTf)_2$, as testified by the absence of variations in its ^{1}H NMR spectrum from −40 °C to 40 °C. Cyclic voltammetry of $(\mathbf{L1})_2$Fe$(OTf)_2$ in CH_3CN (reported in Figure SI 2 in the Supporting Information) exhibits a reversible Fe^{III}/Fe^{II} wave with a redox potential of 1.09 V vs SCE, the high potential being consistent with the expected stabilization of the ferrous state over the ferric state by the π-accepting nature of the pyridine/imine ligand scaffold.

In order to gain insight into the oxidation mechanism of catalyst $(\mathbf{L1})_2$Fe$(OTf)_2$, and to try to tune its activity and selectivity, we targeted the study of $(\mathbf{L2})_2$Fe$(OTf)_2$, $(\mathbf{L3})_2$Fe$(OTf)_2$, and $(\mathbf{L4})_2$Fe$(OTf)_2$ (see Scheme 1), where the electronic properties of the ligand have been varied. $(\mathbf{L2})_2$Fe$(OTf)_2$, $(\mathbf{L3})_2$Fe$(OTf)_2$, and $(\mathbf{L4})_2$Fe$(OTf)_2$ can be prepared by addition of iron(II) triflate to 2 mol equiv of ligands **L2**, **L3**, and **L4**, respectively (see Scheme 1). Ligands **L2**−**L4** are obtained by rapid and quantitative condensation of the corresponding 4-substituted-2-picolyl aldehydes and 2-picolylamine **1** in acetonitrile solution (Scheme 1). Imines **L2**, **L3**, and **L4** bind iron(II) triflate with a 2:1 ligand to iron stoichiometry, as shown by elemental analysis (see Experimental Section) and spectrophotometric titrations in selected cases (see pages SI 16−SI 19 in the Supporting Information). The solid-state structure of $(\mathbf{L3})_2$Fe$(OTf)_2$ obtained by X-ray diffraction (XRD) is reported in the Supporting Information, and it exhibits the same coordination geometry of $(\mathbf{L1})_2$Fe(OTf)(ClO_4), with the two ligands arranged in a meridional fashion around the Fe ion, generating again a slightly distorted octahedral complex. Bond distances are also indicative of a low-spin Fe center, and very much resemble those observed in $(\mathbf{L1})_2$Fe(OTf)(ClO_4). As previously shown for complex $(\mathbf{L1})_2$Fe$(OTf)_2$,[13] complexes $(\mathbf{L2})_2$Fe$(OTf)_2$, $(\mathbf{L3})_2$Fe$(OTf)_2$, and $(\mathbf{L4})_2$Fe$(OTf)_2$ can also be obtained more easily via simple addition in CH_3CN of the corresponding 4-substituted-2-picolylaldehyde to amine **1** and iron(II) triflate in the 2:2:1 ratio directly in the reaction vessel with no prior synthesis required (see Scheme 1 and pages SI 16−SI 19 in the Supporting Information). All complexes show very similar UV-vis spectra (see Figure S4 in the Supporting Information). However, the ^{1}H NMR spectra of crystallized complexes $(\mathbf{L2}-\mathbf{L4})_2Fe(OTf)_2$ are not as simple as expected and show the presence of at least two species (see Figure 2B and Figure S1). Two sets of signals appear as soon as the complex is formed (marked as black squares and triangles in the spectrum of

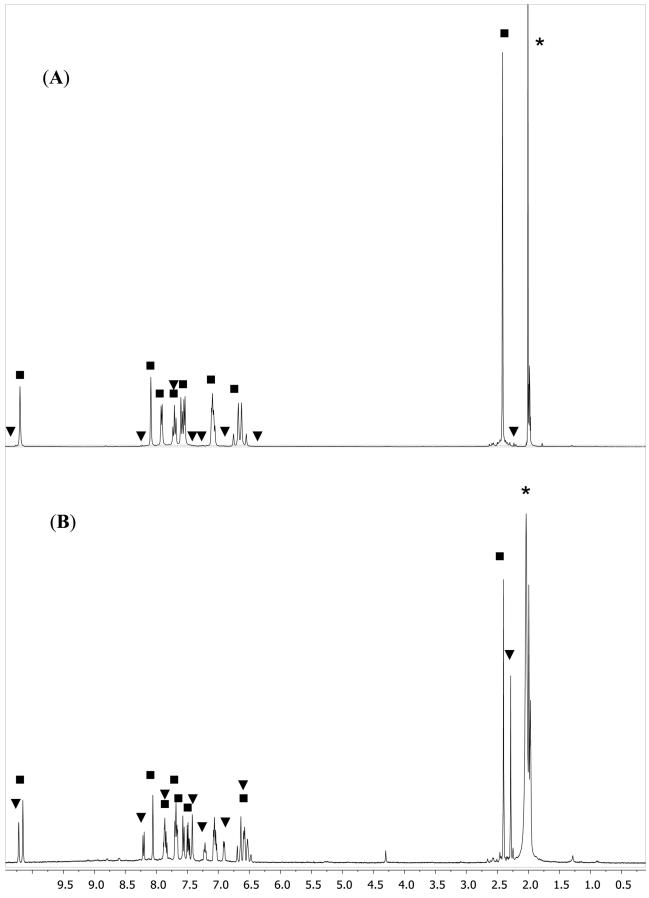

Figure 2. (A) ^{1}H NMR spectrum of $(\mathbf{L3})_2$Fe$(OTf)_2$ in CD_3CN just after its formation. One isomer (marked with black squares, the one depicted on the left in Scheme 2) constitutes the major part of the mixture (ratio = 1:0.08). The minor isomer is marked with black triangles. Solvent and water signals are marked with an asterisk (*). (B) ^{1}H NMR spectrum of $(\mathbf{L3})_2$Fe$(OTf)_2$ in CD_3CN recorded 5 days after its formation in the presence of 5 mol equiv of AcOH (its signal is close to the solvent one). The ratio is now 1:0.85.

$(\mathbf{L3})_2$Fe$(OTf)_2$ reported in Figure 2B), which are not observed in the ^{1}H NMR spectrum of $(\mathbf{L1})_2$Fe$(OTf)_2$ (Figure S1). These two sets of signals very likely arise from the two species displayed in Scheme 2, in which a proton scrambling between

Scheme 2

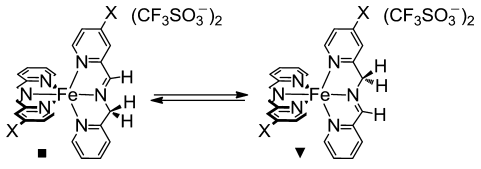

the methylenic and the methinic position is taking place. A similar behavior has been already reported for a closely related Schiff base iron(II) complex.[16] The spectrum of $(\mathbf{L3})_2$Fe$(OTf)_2$ recorded just after the addition of the complex components in solution shows a mixture dominated by one isomer (ratio 1:0.08). A different sample analyzed after longer times from its formation shows a 1:0.35 ratio, which evolves very slowly in the subsequent days. Acetic acid can somewhat accelerate the process (after 5 days, the ratio in the presence of AcOH is 1:0.85 (Figure 2B), whereas, in its absence, the ratio is

DOI: 10.1021/acs.inorgchem.5b01500
Inorg. Chem. XXXX, XXX, XXX−XXX

1:0.37). A complete assignment for $(L3)_2Fe(OTf)_2$ obtained by a COSY experiment is reported in the Supporting Information.

Substituent Effect Studies on Catalytic C−H Oxidation Reactions. Complexes $(L1)_2Fe(OTf)_2$, $(L2)_2Fe(OTf)_2$, $(L3)_2Fe(OTf)_2$, and $(L4)_2Fe(OTf)_2$ were investigated as catalysts in the oxidation of three benchmark hydrocarbon substrates: cyclohexane, adamantane, and (*d*)-menthyl acetate. Catalysts were prepared *in situ*, immediately before carrying out the catalytic oxidations, by reacting picolyl amine **1**, the corresponding picolyl aldehyde, and $Fe(OTf)_2{\cdot}2CH_3CN$ in acetonitrile, in a 2:2:1 ratio. The results are reported in Tables 1, 2, and 3. Control experiments of (*d*)-menthyl acetate oxidation were performed with isolated iron catalysts $(L1)_2Fe(OTf)_2$ and $(L3)_2Fe(OTf)_2$ and provide congruent results, both in terms of yields and selectivities (see Table S5 in the Supporting Information). In cyclohexane oxidation (see Scheme 3 and Table 1), neither total activity, measured in terms of total yield, nor selectivity (A/K ratio) show a clear correlation with the electronic properties of the substituents. A similar situation is observed in adamantane oxidation (Scheme 4 and Table 2) and in (*d*)-menthyl acetate oxidation (Scheme 5 and Table 3). Generally, both electron-withdrawing NO_2 and electron-donating CH_3 lower the catalytic activity of $(L1)_2Fe(OTf)_2$, while OCH_3 has a minor influence. In summary, the electronic nature of the substituent in the *γ*-position on the pyridine ring has a low impact on both the activity and the selectivity of C−H oxidation reactions. This is consistent with the modest substituent effects on C−H oxidations observed with related amine-based nonheme iron catalysts,[17a] and it contrasts with the strong influence on C=C epoxidation activity and selectivity exerted by electronic properties of pyridine rings.[17b]

Mechanistic Studies. The oxidation of the hydrocarbon mechanistic probes shown in Scheme 6 usually enables one to distinguish between a free radical and a metal-based oxidant, as these reactions give significantly different selectivity patterns of products distribution, depending on the mechanistic pathway.[18] The results obtained with catalysts $(L1–L4)_2Fe(OTf)_2$, together with those reported in the literature for related amine-based nonheme iron complexes, are reported in Table 4 for the sake of comparison.

Cyclohexane oxidation was carried out with a large excess of substrate, with respect to the oxidant (100:1) under air. Under these conditions, the large excess of cyclohexane accounts for the preferential oxidation of the latter, with respect to the just-formed cyclohexanol. As a consequence, a high A/K (alcohol/

Scheme 3. Oxidation of Cyclohexane to Cyclohexanol (A) and Cyclohexanone (K)

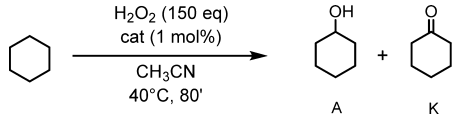

Table 1. Oxidation of Cyclohexane[a]

catalyst	A	K	total	A/K
$(L1)_2Fe(OTf)_2$	14 ± 1	10 ± 1	24	1.4
$(L2)_2Fe(OTf)_2$	14 ± 1	14 ± 1	28	1.0
$(L3)_2Fe(OTf)_2$	9.0 ± 0.5	14 ± 1	23	0.64
$(L4)_2Fe(OTf)_2$	14 ± 1	7.0 ± 0.5	21	0.5

[a]GC yields defined as (mol product/mol substrate) × 100. Reactants: catalyst (1 molar equiv), cyclohexane (100 molar equiv), and hydrogen peroxide (150 molar equiv). Average of three determinations. For further details see Supporting Information.

Scheme 4. Oxidation of Adamantane to 1-Adamantol (A1, 3°), 2-Adamantol (A2, 2°), and Adamantone (K, 2°)

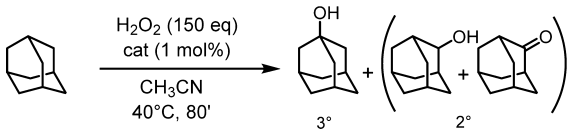

Table 2. Oxidation of Adamantane[a]

catalyst	A1	(A2 + K)	total	3°/2°[b]
$(L1)_2Fe(OTf)_2$	37 ± 1	10 ± 1	47	11
$(L2)_2Fe(OTf)_2$	31 ± 1	8.0 ± 0.5	39	12
$(L3)_2Fe(OTf)_2$	22 ± 1	5.5 ± 0.5	27.5	12
$(L4)_2Fe(OTf)_2$	21 ± 1	7.0 ± 0.5	28	9

[a]See footnote *a* of Table 1. [b]3°/2° is defined as 3 × (1-adamantanol)/(2-adamantanol + 2-adamantanone).

Scheme 5. Oxidation of (*d*)-Menthyl Acetate to Tertiary Alcohol (T1) and Minor Products

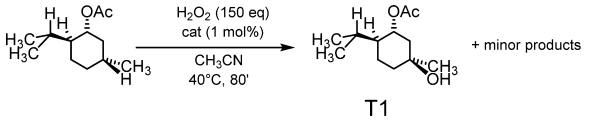

Table 3. Oxidation of (*d*)-Menthyl Acetate[a]

catalyst	T1	total	T1/total	conversion (%)
$(L1)_2Fe(OTf)_2$	20 ± 1	32 ± 1	62%	33
$(L2)_2Fe(OTf)_2$	18 ± 1	26 ± 0.5	69%	29
$(L3)_2Fe(OTf)_2$	16 ± 1	25 ± 1	64%	30
$(L4)_2Fe(OTf)_2$	15 ± 1	29 ± 1	52%	35

[a]See footnote *a* of Table 1.

Scheme 6. Oxidation of Mechanistic Probes Used to Distinguish between a Metal-Based and a Free Radical-Based Oxidation[a]

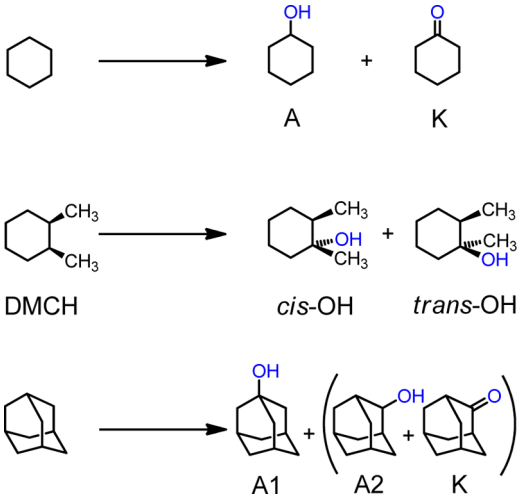

[a]For experimental details, see footnote of Table 4.

DOI: 10.1021/acs.inorgchem.5b01500
Inorg. Chem. XXXX, XXX, XXX−XXX

Table 4. Comparison among Oxidations of Hydrocarbon Probe Substrates Shown in Scheme 6, Catalyzed by (L1−L4)$_2$Fe(OTf)$_2$,[a] Amine-Based Nonheme Iron Complexes and Hydroxyl Radical (HO$^\bullet$)[b]

		Cyclohexane		Adamantane	DMCH	
entry	catalyst	A/K (A + K)[c]	KIE[d]	3°/2°[e]	RC (%)[f]	ref
1	(**L1**)$_2$Fe(OTf)$_2$	11.5 (4.2)	3.3	13	97	this work
2	(**L2**)$_2$Fe(OTf)$_2$	11.7 (5.1)			96	this work
3	(**L3**)$_2$Fe(OTf)$_2$	8.7 (4.0)			93	this work
4	(**L4**)$_2$Fe(OTf)$_2$	8.3 (3.7)			95	this work
5	[(MEN)Fe(OTf)$_2$]	5 (6.3)	3.2	15	96	4b
6	[(TPA)Fe(OTf)$_2$]	6 (3.2)	3.5	17	>99	4b
7	[(^{Me,H}PyTACN)Fe(OTf)$_2$]	12 (6.5)	4.3	30	93	22c
8	α-[(BPMCN)Fe(OTf)$_2$]	9 (5.9)	3.2	15	>99	[redacted]
9	HO$^\bullet$	∼1	∼1	∼2	∼10	19, 20, 21

[a]Reaction conditions: cat:H_2O_2:AcOH:substrate = 1:10:50:1000. Catalyst (10 μmol) prepared *in situ*, 0.40 mL CH_3CN, 40 °C, 80 min. GC yields. All determinations are the average of at least three independent oxidation experiments. [b]Acronyms: MEN, *N*,*N*′-dimethyl-*N*,*N*′-bis(2-picolyl)ethane-1,2-diamine; TPA, trispicolylamine; ^{Me,H}PyTACN, 1,4-dimethyl-7-(2-picolyl)-1,4,7-triazacyclononane; and BPMCN, *N*,*N*′-bis(2-picolyl)-cyclohexane-*trans*-1,2-diamine. [c]Turnover number (TON) (mol of product/mol of catalyst). A = cyclohexane, K = cyclohexanone. One thousand mol equiv of cyclohexane. [d]KIE measured in the competitive oxidation of a 1:3 mixture of cyclohexane/cyclohexane-d_{12}. Total 1 mmol of substrates. [e]3°/2° = 3 × (1-adamantanol)/(2-adamantanol + 2-adamantanone). 100 μmol of adamantane, 180 min. [f]RC = 100 × (*cis*-OH − *trans*-OH)/(*cis*-OH + *trans*-OH).

ketone) ratio is found for metal-based oxidants. On the other hand, if the reaction involves a free-radical process, equimolar amounts of alcohol and ketone (A/K ≈ 1) are usually observed, because of Russell-type terminations.[19] With catalyst (**L1**)$_2$Fe(OTf)$_2$, we observed a high A/K ratio of 11.5 (Table 4, entry 1), which was unaffected by the rate of hydrogen peroxide addition.[20] Comparable values (Table 4, entries 2−4) are obtained also for the other complexes of the series, indicating the involvement of a selective metal-based oxidant. Also, the intermolecular KIE value (3.3) measured in a competitive cyclohexane/cyclohexane-d_{12} oxidation is a clue for a selective oxidant, being able to discriminate between C−H and C−D bonds (difference of 1.7 kcal mol^{-1}). In fact, reactions initiated by hydroxyl radicals usually give KIE values between 1 and 2.[21a,b] The KIE in such reactions is indicative only of the selectivity-determining step; thus, it allows one to distinguish selective oxidants from highly reactive hydroxyl radicals.[21c] All the above values are consistent with those obtained with other nonheme amine-based iron complexes reported in the literature (A/K values are in the range of 5−12, KIE values are in the range of 3.2−4.3, entries 5−8 in Table 4) for which the involvement of a metal-based oxidant has been accepted, and differ substantially from those observed in reactions initiated by HO$^\bullet$. The formation of cyclohexyl hydroperoxide may constitute an additional indication for free-radical reactions. Analysis with the Shul'pin method[24] showed that no significant amounts of cyclohexyl hydroperoxide are formed in cyclohexane oxidation catalyzed by (**L1**)$_2$Fe(OTf)$_2$ (see Table S6 in the Supporting Information). Furthermore, when the oxidation of cyclohexane was performed under argon, no significant variation of the reaction selectivity was observed, again arguing against a radical-based oxidation (see Table S7 in the Supporting Information).

Consistent with the above results, the selectivity pattern obtained in adamantane oxidation is also indicative of a metal-based oxidant. We measured a 3°/2° ratio of 13 (see Table 4), which, although slightly lower, is far more similar to 3°/2° ratios obtained with other nonheme iron complexes (3°/2° = 15−30) than to those obtained with HO$^\bullet$ radical (3°/2° ratio of ∼2).[22,23] Eventually, the high level (97%) of stereoretention in 1,2-*cis*-dimethylcyclohexane oxidation is definitive evidence in favor of the involvement of a metal-based oxidant rather than a free-radical oxidation, for which a much lower stereoretention must be expected, because of the fast epimerization of the radical intermediate ($t_{1/2}$ ≈ 10^{-9} s).[4b,22,23] Such high values of retention of configuration are found also for the other complexes along the series (see Table 4).

To gain a deeper insight into the oxidation process, we studied the origin of the oxygen atom incorporated in the products by means of isotopic labeling experiments. In principle, the O atom incorporated in the oxidized substrate can be derived from H_2O_2, H_2O, or molecular oxygen (O_2). As reported above, cyclohexane oxidation carried out under argon or under air gave similar results, thus excluding O_2 as the oxygen source. We measured the amount of ^{18}O incorporation in secondary and tertiary C−H bond oxidation (Scheme 7)

Scheme 7. Oxidation of Secondary and Tertiary C−H Catalyzed by (L1)$_2$Fe(OTf)$_2$ in the Presence of $H_2{}^{16}O_2$ and $H_2{}^{18}O$ or *Vice Versa*

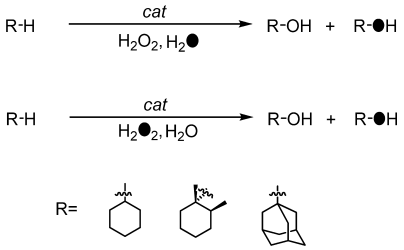

catalyzed by (**L1**)$_2$Fe(OTf)$_2$ in the presence of 10 equiv of $H_2{}^{16}O_2$ and 1000 equiv of $H_2{}^{18}O$ (entries 1−4 of Table 5).[25] No ^{18}O incorporation from labeled water was observed in all cases, even when varying the amount of $H_2{}^{18}O$ (entries 5 and 6 of Table 5). Complementary experiments were performed with $H_2{}^{18}O_2$ and $H_2{}^{16}O$ in the oxidation of 1,2-*cis*-dimethylcyclohexane and cyclohexane (entries 7 and 8 of Table 5). In this case, 96% and 80% ^{18}O incorporations in 1,2-*cis*-dimethylcyclohexane and cyclohexane oxidation, respectively, were observed. The small but still significant incorporation of O_2 in the oxidation reactions indicates that (i) a minor path involving the formation of alkyl radicals is also participating in the reaction,

DOI: 10.1021/acs.inorgchem.5b01500
Inorg. Chem. XXXX, XXX, XXX−XXX

Table 5. Percentage of ^{18}O Incorporation in Secondary and Tertiary C−H Bond Oxidation Promoted by $(L1)_2Fe(OTf)_2$[a]

entry	substrate	equivalents of substrate	^{18}O source	% incorporation
1	1,2-*cis*-dimethylcyclohexane	100	$H_2{}^{18}O$	0
2	adamantane[b]	10	$H_2{}^{18}O$	0
3	cyclohexane	1000	$H_2{}^{18}O$	<1
4	cyclohexane	100	$H_2{}^{18}O$	<1
5	cyclohexane[c]	100	$H_2{}^{18}O$	<1
6	cyclohexane[d]	100	$H_2{}^{18}O$	<1
7	1,2-*cis*-dimethylcyclohexane	100	$H_2{}^{18}O_2$	96
8	cyclohexane	100	$H_2{}^{18}O_2$	80

[a]Experimental details as described in footnote *a* of Table 4. $H_2{}^{18}O$ (1000 equiv) was added. Reactions performed under air. GC-MS analysis. All determinations are the average of at least two independent oxidation experiments. [b]Because of solubility problems, the total volume of the reaction mixture was 1.0 mL. [c]660 equiv of $H_2{}^{18}O$ were added. [d]2000 equiv of $H_2{}^{18}O$ were added.

and (ii) this path is somewhat more significant in the oxidation of cyclohexane.

Substantial O atom incorporation from water is usually observed in iron complexes containing two *cis* labile sites, because of a rapid oxo-hydroxo tautomerism of the high valent iron-oxo intermediate.[3a,4b,6] The absence of water O atom incorporation with complex $(L1)_2Fe(OTf)_2$ bears some mechanistic considerations. First, it suggests that the actual oxidizing iron species cannot coordinate both hydrogen peroxide and a water molecule simultaneously. This hypothesis is strengthened by the observation that acetic acid hardly affects reaction yields and selectivities (see Table S7 in the Supporting Information). Acetic acid has a beneficial effect for tetradentate iron complexes, and it is proposed to play a similar role as the water molecule, by coordinating to iron adjacent to the peroxide moiety, and assisting O−O bond heterolysis.[4,5a,26] An additional observation suggesting that a water-assisted O−O lysis is not occurring arises from the observation that catalytic cyclooctene oxidation catalyzed by $(L1)_2Fe(OTf)_2$ only produces epoxide and no *cis*-diol is detected (see Table S7). *cis*-Dihydroxylation has been shown to require two *cis*-labile sites at the Fe site, because of the proposed involvement of the Fe(O)(OH) intermediate as the active oxidant.[4a,6,27] The absence of traces of *cis* diols argues against the formation of this high valent Fe(O)(OH) intermediate in oxidations mediated by $(L1)_2Fe(OTf)_2$, even in the case that such an intermediate is too reactive to engage in the oxo-hydroxo tautomerism. Therefore, $(L1)_2Fe(OTf)_2$ must activate H_2O_2 and form a selective C−H hydroxylating species via a reaction mechanism that departs from the one operating in iron complexes with tetradentate aminopyridine ligands. A second element that deserves consideration is the fact that water incorporation into oxidation products is commonly taken as an indication of the implication of high valent iron-oxo species in oxidation reactions.[4b,6] However, the lack of water incorporation does not exclude the implication of the latter species in C−H oxidation reactions. It is also possible that they form, but the rate of water exchange is much smaller than reaction with the substrate.

Complex $(L1)_2Fe(OTf)_2$ is hexacoordinated, so it should either expand its coordination sphere to become heptacoordinated, or detach one ligand arm opening a site on the Fe ion for H_2O_2 binding and activation. To discriminate between these two pathways, complex $(terpy)_2Fe(OTf)_2$,[28] which is structurally similar to $(L1)_2Fe(OTf)_2$, has been studied. The high rigidity of terpyridine ligand should strongly disfavor the detachment of one pyridine arm from the Fe center, but it should not affect the possibility of opening a seventh coordination site. Complex $(terpy)_2Fe(OTf)_2$ shows no activity at all in C−H bond oxidation (see Table S7), and the purple color of the solution remains unaltered upon H_2O_2 addition, again indicating that no reaction is taking place. These results point to the former H_2O_2 coordination mechanism. To check if the trend is correct, complex $(L5)_2Fe(OTf)_2$ was also prepared, with an intermediate rigidity between $(L1)_2Fe(OTf)_2$ and $(terpy)_2Fe(OTf)_2$, because of the presence of two methyl groups. Complex $(L5)_2Fe(OTf)_2$ and ligand **L5**[29] were obtained following the same procedure used for the other imine complexes (see Scheme 8 and pages SI 21 and SI 22 in the Supporting Information). Indeed, $(L5)_2Fe(OTf)_2$ exhibits a catalytic activity that is much lower than that of complexes $(L1-L4)_2Fe(OTf)_2$ (compare Table S7 with Tables 1−3), but still higher than $(terpy)_2Fe(OTf)_2$.

Scheme 8. Relationship bewteen Catalytic Activity and Rigidity in Ligands Used in This Study[a]

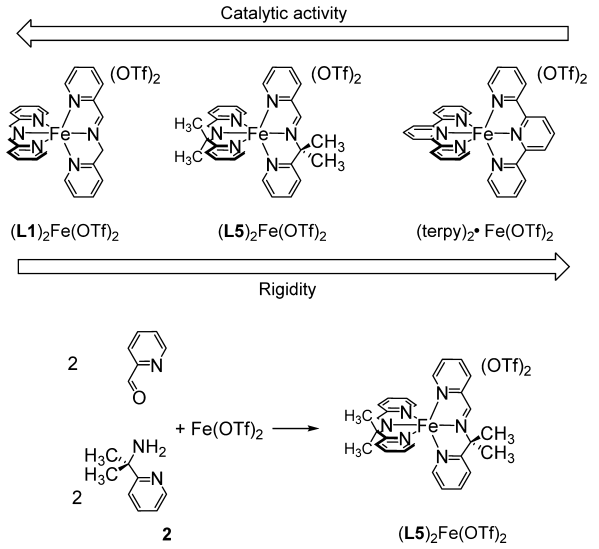

[a]Here, terpy = 2,2′-6,6′-terpyridine.

To rationalize these observations, we propose that ligand flexibility has a remarkable impact on catalytic activity (Scheme 8), with the more-rigid ligands decreasing or even shutting down the reaction. A high degree of ligand flexibility is probably needed for an efficient undocking of one pyridine arm. On this basis, it seems plausible that the active species of $(L1)_2Fe$ loosens the coordination of a pyridine arm and opens a free site on the Fe, generating a pentadentate complex where the sixth position can be then ready for reaction with hydrogen peroxide.

Alternative scenarios entailing oxidative degradation of the ligand, eventually leading to iron species with unsaturated coordination spheres were also considered. The evolution of complex $(L1)_2Fe(OTf)_2$ during adamantane oxidation was investigated by monitoring the reaction using electrospray ionization−mass spectroscopy (ESI-MS) (Figure 3). Initially, the mixture is dominated by two main peaks attributed to

DOI: 10.1021/acs.inorgchem.5b01500
Inorg. Chem. XXXX, XXX, XXX−XXX

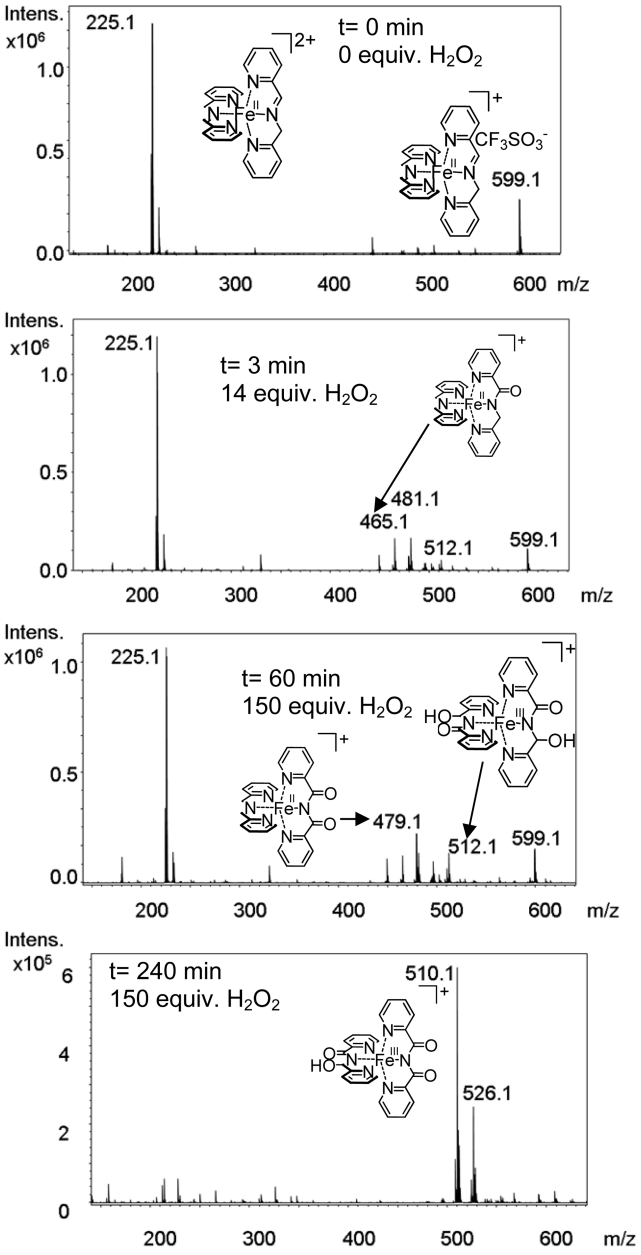

Figure 3. ESI-MS spectra evolution of the mixture during adamantane oxidation catalyzed by $(\mathbf{L1})_2Fe(OTf)_2$ in the presence of the given amount of H_2O_2.

complex $(\mathbf{L1})_2Fe(OTf)_2$ on the basis of HRMS analysis (see Figure SI 17 in the Supporting Information): one at m/z = 225, which is assigned to doubly charged $(\mathbf{L1})_2Fe^{2+}$, and one at m/z = 599, which is assigned to $(\mathbf{L1})_2Fe(OTf)^+$. When H_2O_2 was slowly added by a syringe pump, the peak at m/z = 599 gradually decreases in intensity, while new peaks appear in the region of m/z = 465−512, which were attributed to products arising from oxidation of the picolinic methylenes of ligand **L1** (for a tentative complete assignment of peaks, see Figure SI 18 in the Supporting Information). Scheme 9 shows some possible oxidation products of $(\mathbf{L1})_2Fe(OTf)_2$. Oxidation of amino-pyridine ligand at picolinic positions has been already reported for related iron complexes. Bauer obtained spectrometric evidence that the saturated *bis* amine analogue of complex $(\mathbf{L1})_2Fe^{2+}$ is oxidized by H_2O_2 to $((\mathbf{L7})_2Fe^{III})^+$ (see Chart 1),[12a] while Mascharak and co-workers[30] observed that the iron

Scheme 9. Example of the Oxidative Pathway from $(\mathbf{L1})_2Fe(OTf)_2$ and Corresponding Molecular Masses

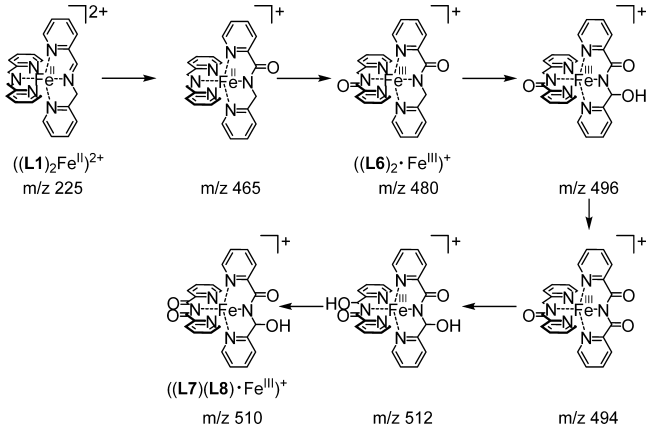

Chart 1

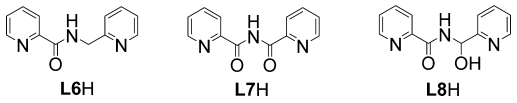

amide complex $(\mathbf{L6})_2Fe^{II}(OTf)_2$ is rapidly oxidized to $(\mathbf{L6})_2Fe^{III}$ by exposure to air. In our case, the ligands **L1** in complex $(\mathbf{L1})_2Fe^{2+}$ are increasingly oxidized as H_2O_2 addition proceeds, going from imine **L1** to monoamide **L6** and, eventually, to oxidized imide **L7**, with the oxidation state of Fe changing from Fe(II) to Fe(III). However, compared to peaks related to complex $(\mathbf{L1})_2Fe^{2+}$, the intensity of peaks due to the latter species remains modest throughout oxidant addition, with the peak at m/z = 225 being the major peak, even when 150 equiv of H_2O_2 are added. Only 4 h after the beginning of the reaction, the ESI-MS spectra show a prominent peak at m/z = 510, attributed to the oxidized species $((\mathbf{L7})(\mathbf{L8})\cdot Fe^{III})^+$ depicted in Scheme 9. Interestingly, peaks that could indicate the formation of picolinic acid, which is a well-known ligand in iron-catalyzed oxidations,[31] are not observed.

The results of the mass analysis are consistent with the UV-vis monitoring of the solution, during adamantane oxidation, which provides more quantitative insight. Results are shown in Figure 4. Complex $(\mathbf{L1})_2Fe^{2+}$ is the predominant form of iron (80% of the initial concentration based on ε) during the first 30 min of reaction, and it is still present, although in a lower amount (20% based on ε), even after 3 h of reaction.

In order to check if the oxidized species observed in the ESI-MS spectrum are active oxidants or inactive catalyst degradation products, we independently prepared amide ligand **L6H**[30] (see pages S13, S25, and S26 in the Supporting Information) and tested the efficiency of a 2:1 **L6**H:$Fe(OTf)_2$ mixture as a catalyst of C−H bond oxidations of cyclohexane and adamantane under the same reaction conditions employed in the reactions catalyzed by $(\mathbf{L1})_2Fe(OTf)_2$. The low product yields determined in these experiments (see Table S7) clearly indicate that oxidation byproducts such as $(\mathbf{L6})_2Fe^{II}$ or $(\mathbf{L6})_2Fe^{III}$ or the complexes derived from their subsequent oxidation cannot be responsible for the catalytic activity observed with $(\mathbf{L1})_2Fe(OTf)_2$. We conclude that the species observed in the ESI-MS spectrum with m/z comprised between m/z = 481 and 510 are oxidative degradation products of $(\mathbf{L1})_2Fe(OTf)_2$ that lie along the catalyst deactivation pathway.

DOI: 10.1021/acs.inorgchem.5b01500
Inorg. Chem. XXXX, XXX, XXX−XXX

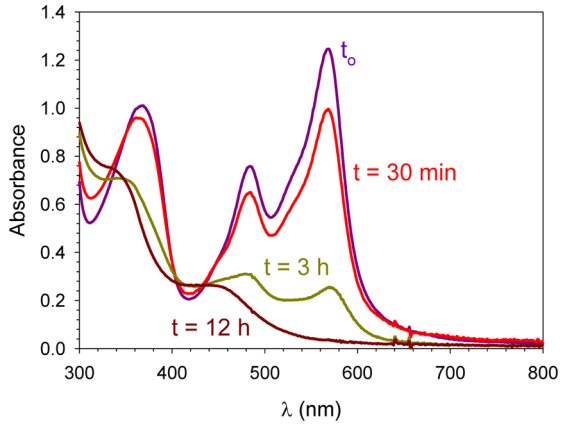

Figure 4. Time-resolved UV-vis spectra recorded in the oxidation of adamantane with H_2O_2 catalyzed by $(\mathbf{L1})_2Fe(OTf)_2$. Conditions: $(\mathbf{L1})_2Fe(OTf)_2$ 0.15 mM, [adamantane] 15.0 mM, [H_2O_2] = 3 mM. Spectrum t_o has been recorded before the addition of hydrogen peroxide.

An induction period of 20 min was observed in the case of adamantane oxidation (see Figure 5),[32] and this observation

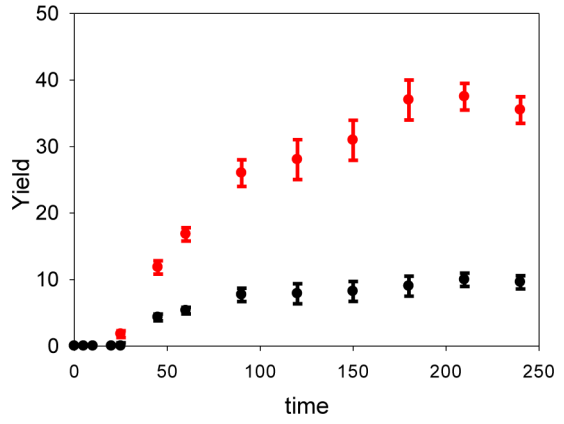

Figure 5. Time profile of product yields in the oxidation of adamantane with H_2O_2 catalyzed by $(\mathbf{L1})_2Fe(OTf)_2$. Legend: red circles, yield of 1-adamantanol; black circles, 2-adamantanol and 2-adamantanone. Reaction conditions: $(\mathbf{L1})_2Fe(OTf)_2$ (1.13 μmol, 1 equiv), H_2O_2 (170 μmol, 150 equiv), adamantane (113 μmol, 100 equiv) in CH_3CN at 40 °C.

points to $(\mathbf{L1})_2Fe(OTf)_2$ being a precatalyst, which is converted to an active form during the first minutes of reaction. This fact is strengthened by the modest but measurable increase in total yield on increasing preexposure time of $(\mathbf{L1})_2Fe(OTf)_2$ to hydrogen peroxide before substrate addition (see Figure S21 in the Supporting Information).

Two mechanistic pathways may be initially taken into account. The first one considers catalyst $(\mathbf{L1})_2Fe^{II}(OTf)_2$ cycling from an Fe(II) oxidation state to an Fe(IV) oxidation state, as suggested for other nonheme iron complexes by Que and Comba.[33] This hypothesis may explain the lack of active Fe(III) species both in ESI-MS and in UV-vis spectra, but it does not account for the observed lag time. The second mechanistic pathway is based on hydrogen peroxide activation at a Fe(III) center, akin to that proposed for aminopyridine iron complexes, with an initial rate-determining oxidation of $(\mathbf{L1})_2Fe^{II}$ to $(\mathbf{L1})_2Fe^{III}$ by H_2O_2. The more labile Fe(III) complex may rapidly detach one pyridine arm, allowing H_2O_2 coordination and subsequent activation. After a number of rapid cycles, the catalyst is subjected to oxidative degradation pathways and deactivates.

In order to discard one of the above two hypotheses, we checked if the induction period in adamantane oxidation is observed, even when $(\mathbf{L1})_2Fe^{II}$ is oxidized to Fe(III) before H_2O_2 addition. With this aim, we replaced $Fe^{II}(OTf)_2$ with $Fe^{III}(OTf)_3$ in the preparation of a $(\mathbf{L1})_2Fe$ complex (see page S33 in the Supporting Information) and employed it as catalyst for adamantane oxidation. The reaction time profile is reported in Figure 6 (details given in Table S9 in the Supporting

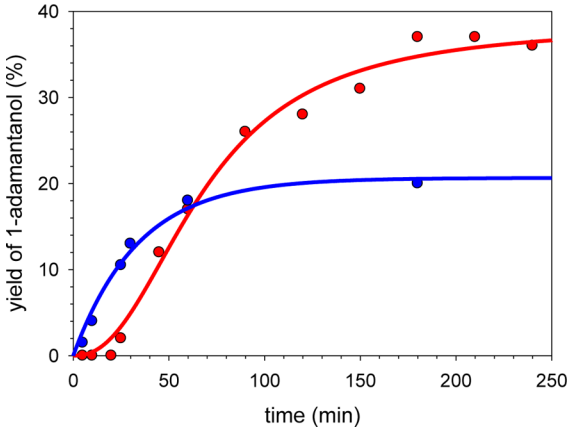

Figure 6. Time profile of 1-adamantanol yield in adamantane oxidation catalyzed by $(\mathbf{L1})_2Fe^{II}(OTf)_2$ (red circles and red curve) or by $(\mathbf{L1})_2Fe^{III}(OTf)_3$ (blue circles and blue curve). Reaction conditions as in the caption of Figure 4.

Information). Using $(\mathbf{L1})_2Fe^{III}(OTf)_3$, no induction period was detected, showing an exponential-type product accumulation. However, the total yield of the reaction is definitely lower, probably because of a faster deactivation. Also, *in situ* oxidation of $(\mathbf{L1})_2Fe^{II}(OTf)_2$ to $(\mathbf{L1})_2Fe^{III}$ with a strong one-electron oxidant (namely, $[Ru(bpy)_3](ClO_4)_3$, $E_{1/2}$= 1.26 V vs SCE[34]) before substrate and H_2O_2 addition leads to the disappearance of the lag time (see Table S8). Increasing the ligand/metal ratio to 3:1 leads to longer induction times, while decreasing this ratio to 1:1 gives rise to less-selective reactions, as testified by the lower 3°/2° ratios and the lower yields (see Table S9). Therefore, we can conclude that the most likely mechanistic pathway involves initial one-electron oxidation of $(\mathbf{L1})_2Fe^{II}$ as the rate-determining step in the catalytic cycle.

SUMMARY AND CONCLUSIONS

Imine-based complex $(\mathbf{L1})_2Fe(OTf)_2$ effectively oxidizes non-activated C–H bonds at low catalyst loading (1%). Its main advantage lies in the great ease of preparation, as it is synthesized just by mixing $Fe(OTf)_2$, 2-picolylaldehyde, and 2-picolylamine **1** in a 1:2:2 ratio directly in the reaction vessel, with no prior isolation required. The latter feature makes such catalysts competitive with several more studied amine-based nonheme iron complexes (*vide supra*). Systematic variation of complex pyridine γ-substituents electronic properties has a very low impact on both catalytic activity and selectivity.

From a mechanistic perspective, complex $(\mathbf{L1})_2Fe(OTf)_2$ clearly operates via a selective, metal-based oxidant, as shown by the typical selectivity patterns in mechanistic probe oxidations and from the high retention of configuration (97%) in 1,2-*cis*-dimethylcyclohexane hydroxylation. Labeling

DOI: 10.1021/acs.inorgchem.5b01500
Inorg. Chem. XXXX, XXX, XXX–XXX

Scheme 10. First Transformations in the Catalytic Cycle of $(L1)_2Fe(OTf)_2$, Showing the Conversion of the Precatalyst into the Catalyst and Hydrogen Peroxide Coordination

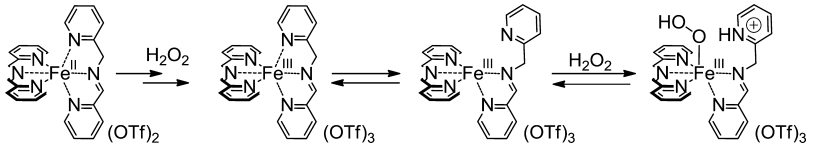

experiments demonstrated that H_2O_2 is the O-atom source, with minimum incorporation from H_2O or O_2. This observation, together with other indirect experimental clues, points toward H_2O_2 activation taking place at an iron species with a single coordination site available. Since all six sites are occupied by the two ligand molecules, one pyridine arm must detach to bind and activate H_2O_2. Indeed, any increase in ligand rigidity causes a significant loss of catalytic activity, confirming that a high degree of ligand flexibility is required to start the catalytic cycles. However, the detached pyridine should remain bound to the ligand, because all products observed in the ESI-MS contain the entire ligand. The pyridine detached arm may possibly be protonated and assist O−O bond cleavage by a pull effect, similar to the ammonium arm assistance proposed by Rybak-Akimova for a different nonheme iron complex.[35] This PyH^+ assistance may explain the unusual high catalytic activity of complex $(L1)_2Fe(OTf)_2$ when compared to the low activity usually reported for related amine-based pentadentate iron catalysts.[36] Based on the collected data, a mechanism for the first steps of the catalytic cycle has been proposed, and it is summarized in Scheme 10. The onset of catalytic activity requires oxidation of $(L1)_2Fe^{II}$ to $(L1)_2Fe^{III}$, as demonstrated by the disappearance of the lag time if $(L1)_2Fe^{II}$ is replaced with $(L1)_2Fe^{III}$. Subsequently, the $(L1)_2Fe^{III}$ intermediate rapidly detaches one pyridine arm and enters in the catalytic cycle by binding and activating H_2O_2, until it eventually undergoes oxidative degradation and subsequent catalyst deactivation. Interpretation of the exact nature of the oxidant species that form upon H_2O_2 activation at $(L1)_2Fe^{III}$ deserves some caution. Imine ligands are usually regarded as readily oxidizable (with the notable exception of salen-type ones) and usually favor low oxidation states of the metal; therefore, it appears highly unlikely that an iron center in a high oxidation state (Fe^V)[37] could be supported by an imine ligand. An alternative possibility is that iminopyridine ligand moieties act as red-ox non innocent molecules that accumulate oxidizing equivalents in a cyt P450-like manner.[38] While the precise nature of the active species could not be ascertained, $(L1)_2Fe^{II}$ constitutes the first example of an imine-based iron complex that can mediate hydroxylation of alkanes via a metal-based oxidant. Further studies are ongoing in order to expand the scope of this catalytic oxidation, and to elucidate the nature of the oxidizing species.

EXPERIMENTAL SECTION

Instruments and General Methods. Oxidation products were identified by comparison of their GC retention times and GC/MS with those of authentic compounds and/or by ^1H NMR analyses. GC analyses were carried out on a gas chromatograph equipped with a capillary methylsilicone column (30 m × 0.25 mm × 25 μm, Chrompack CP-Sil 5 CB). GC-MS analyses were performed with a mass detector (EI at 70 eV) coupled with a gas chromatograph equipped with a melted silica capillary column (30 m × 0.2 mm × 25 μm) covered with a methylsilicone film (5% phenylsilicone, OV5). NMR spectra were recorded on a spectrometer (either Bruker Model DPX300 or Bruker Model DPX400) and were internally referenced to the residual proton solvent signal. UV-vis spectra were registered by a double-ray spectrophotometer (Perkin, Model Lambda 18). Elemental analyses were performed using a CHNS-O EA-1108 elemental analyzer from Fisons. Electrospray ionization mass spectrometry (ESI-MS) experiments were performed on a Bruker Daltonics Esquire 6000 Spectrometer using solutions >1 mM of the analyzed compound. High-resolution mass spectra (HRMS) were recorded on a Bruker MicroTOF-Q IITM instrument with an ESI source at Serveis Tècnics of the University of Girona. Samples were introduced into the mass spectrometer ion source by direct infusion through a syringe pump and were externally calibrated using sodium formate. Cyclic voltammetric (CV) experiments were performed in an IJ-Cambria IH-660 potentiostat using a three-electrode cell. Glassy carbon disk electrode (3 mm diameter) from BAS were used as the working electrode, platinum wire was used as auxiliary, and SSCE was used as the reference electrode (all the potentials given in this work are always with regard to this reference electrode). All cyclic voltammograms were recorded at a scan rate of 100 mV s^{-1}. The complexes were dissolved in previously degassed solvents containing the necessary amount of n-Bu_4NPF_6 as supporting electrolyte to yield a 0.1 M ionic strength solution. All $E_{1/2}$ values reported in this work were estimated from cyclic voltammetric experiments as the average of the oxidative and reductive peak potentials $(E_{pa} + E_{pc})/2$.

Materials. All reagents and solvents were purchased from Sigma−Aldrich and were reagent grade, unless otherwise stated. Solvents used for crystallizations were purchased from SDS and Scharlab and were purified and dried by passing through an activated alumina purification system (M-Braun SPS-800) or by conventional distillation techniques. Sigma−Aldrich high-performance liquid chromatography (HPLC)-grade acetonitrile was employed for oxidation reactions. Iron(II) bis-(trifluoromethanesulfonate) bis-(acetonitrile) was prepared according to a literature procedure from Fe(II) chloride (Sigma−Aldrich).[39] 2-picolyl aldehyde, 4-methyl-2-picolyl aldehyde, 2-picolylamine **1**, amine **2**, 2-picolinic acid, terpyridine, acetic acid, and (*d*)-menthyl acetate were purchased from Sigma−Aldrich and used as received. Adamantane was purchased from Fluka. Cyclohexane and 1,2-*cis*-dimethyl cyclohexane were purchased from Sigma−Aldrich and filtered over SiO_2 before use. 4-Methoxy-2-picolyl aldehyde and 4-nitro-2-picolyl aldehyde were synthesized following a literature procedure.[40] Ligand **L6H** was prepared according to a published procedure.[30]

Synthesis of Ligands. Synthesis of ligand **L1** has been already described in a previous paper.[13]

Ligands **L2**, **L3**, and **L4** were prepared by mixing equimolar amounts of 2-picolylamine **1** and 4-methoxy-2-formylpyridine, 4-methyl-2-formylpyridine, or 4-nitro-2-formylpyridine, respectively, in CH_3CN at room temperature. Reactions are quantitative as demonstrated by ^1H NMR analysis. Ligand solution were taken to dryness and used without further purification.

Ligand **L2**. Ligand **L2** was prepared by mixing 450 μL of a solution 0.510 M of 4-methoxy-2-formylpyridine in CH_3CN with 460 μL of a 2-picolylamine **1** 0.496 M solution in CH_3CN at room temperature. ^1H NMR (300 MHz, CD_3CN, 25 °C) δ: 8.55 (m, 1H), 8.50 (m, 1H), 8.46 (m, 1H), 7.75 (m, 1H), 7.57 (m, 1H), 7.45 (m, 1H), 7.26 (m, 1H), 7.96 (m, 1H), 4.94 (s, 2H), 3.89 (s, 3H). ^{13}C NMR (300 MHz, CD_3CN) δ: 166.2, 163.9, 158.9, 156.4, 150.7, 149.3, 136.8, 122.38, 122.22, 111.9, 105.4, 66.0, 55.2. HRMS (ESI-TOF) for $C_{13}H_{13}N_3ONa$: calcd, 250.0951 ($M + Na^+$); found, 250.0951.

DOI: 10.1021/acs.inorgchem.5b01500
Inorg. Chem. XXXX, XXX, XXX−XXX

Ligand L3. Ligand **L3** was prepared by mixing 480 μL of a solution 0.474 M of 4-methyl-2-formylpyridine in CH_3CN with 440 μL of a 2-picolylamine **1** 0.520 M solution in CH_3CN at room temperature. ^1H NMR (400 MHz, CD_3CN, 25 °C) δ: 8.55 (d, 1H, J = 4 Hz), 8.52 (m, 2H), 8.57 (m, 2H), 7.89 (s, 1H), 7.76 (td, 1H, 2J = 8 Hz, 1J = 4 Hz), 7.45 (d, 1H, J = 8 Hz), 7.26 (m, 2H), 4.94 (s, 2H), 2.39 (s, 3H). ^{13}C NMR (400 MHz, CD_3CN) δ: 165.5, 160.4, 155.9, 150.7, 149.6, 138.2, 127.4, 123.8, 123.7, 122.7, 67.6, 21.5. HRMS (ESI-TOF) for $C_{13}H_{13}N_3Na$: calcd, 234.1002 (M + Na^+); found, 234.0996.

Ligand L4. Ligand **L4** was prepared by mixing 405 μL of a solution 0.564 M of 4-nitro-2-formylpyridine in CH_3CN with 440 μL of a 2-picolylamine **1** 0.520 M solution in CH_3CN at room temperature. ^1H NMR (300 MHz, CD_3CN, 25 °C) δ: 8.97 (m, 1H), 8.67 (m, 1H), 8.57 (m, 2H), 8.10 (m, 1H), 7.78 (m, 1H), 7.51 (m, 1H), 7.27 (m, 1H), 5.02 (s, 2H), 3.89 (s, 3H). ^{13}C NMR (300 MHz, CD_3CN) δ: 162.1, 158.4, 157.4, 152.0, 149.3, 136.8, 122.47, 122.35, 113.1, 65.9. HRMS (ESI-TOF) for $C_{12}H_{10}N_4O_2Na$: calcd, 265.0696 (M + Na^+); found, 265.0690.

Synthesis of Complexes. *Complex (L1)$_2$Fe(OTf)$_2$.* 1.39 mL of a 0.264 M CH_3CN solution of ligand **L1** (366 μmol) was added to 80.0 mg (183 μmol) of $Fe(OTf)_2(CH_3CN)_2$ under a N_2 atmosphere. The solution was stirred for 30 min, and the solvent was removed under reduced pressure. The dark purple solid was redissolved into anhydrous CH_3CN and filtered over Celite; then, crystals were obtained by slow diffusion of Et_2O (84 mg, 61% yield). X-ray-quality crystals were grown by slow diffusion of diethyl ether into acetonitrile or dichloromethane solutions of 1:2 mixtures of $(\mathbf{L1})_2Fe(OTf)_2$ and $NaClO_4$. Complex $(\mathbf{L1})_2Fe(OTf)_2$ can be prepared also by mixing $Fe(OTf)_2(CH_3CN)_2$, 2-formylpyridine, and 2-picolylamine **1** in a 1:2:2 molar ratio (respectively) in CH_3CN solution, as demonstrated previously.[13] ^1H NMR (400 MHz, CD_3CN, 25 °C) δ: 10.20 (s, 2H), 8.20 (d, 2H, J = 8 Hz), 7.86 (m, 5H), 7.68 (m, 5H), 7.56 (d, 2H, J = 8 Hz), 7.21 (t, 2H, J = 8 Hz), 6.60 (dd, 4H, J = 24 Hz). HRMS (ESI-TOF) for $C_{25}H_{22}N_6O_3F_3SFe$: calcd, 599.0770 (M + OTf); found, 599.0769. Elemental analysis for $C_{26}H_{22}N_6O_6F_6S_2Fe$ ($(\mathbf{L1})_2Fe(OTf)_2$): calcd: C, 41.72, H, 2.96, N, 11.23; found: C, 41.99, H, 2.98, N, 11.45. UV-vis: λ 369 nm (ε = 7800), λ 484 nm (ε = 5500), λ_{max} 566 nm (ε = 9500).

Complex (L2)$_2$Fe(OTf)$_2$. 730 μL of a 0.252 M CH_3CN solution of ligand **L2** (183 μmol) were added to 40.0 mg (91.7 μmol) of $Fe(OTf)_2(CH_3CN)_2$ under a N_2 atmosphere. The solution was stirred for 30 min and the solvent was removed under reduced pressure. The dark purple solid was redissolved into anhydrous CH_2Cl_2 and filtered over Celite, and then crystals were obtained by slow diffusion of Et_2O (55 mg, 74% yield). Complex $(\mathbf{L2})_2Fe(OTf)_2$ can be prepared also by mixing $Fe(OTf)_2(CH_3CN)_2$ 4-methoxy-2-formylpyridine and 2-picolylamine **1** in a 1:2:2 molar ratio in CH_3CN solution, as demonstrated by the UV-vis spectra (see pages S16 and 17 in the Supporting Information). ^1H NMR (400 MHz, CD_3CN, 25 °C) δ: 10.24 (s, 2H), 10.13 (s, 2H), 8.21 (d, 2H, J = 8 Hz), 7.83 (m, 6H), 7.68 (m, 4H), 7.56 (d, 4H, J = 8 Hz), 7.37 (m, 2H), 7.22 (m, 2H), 7.18 (m, 2H), 7.04 (m, 2H), 6.79 (m, 2H), 6.59 (m, 10H), 3.86 (s, 6H), 3.79 (s, 6H). HRMS (ESI-TOF in MeOH) for $C_{27}H_{29}N_6O_3Fe$: calcd, 541.1651 ($(\mathbf{L2})_2Fe(OMe)$); found, 541.1599. Elemental analysis for $C_{28}H_{26}N_6O_8F_6S_2Fe$ ($(\mathbf{L2})_2Fe(OTf)_2$): calcd: C, 41.60, H, 3.24, N, 10.39; found: C, 41.45, H, 3.54, N, 10.88. UV–vis: λ 374 nm (ε = 9000), λ 482 nm (ε = 5600), λ_{max} 566 nm (ε = 9900).

Complex (L3)$_2$Fe(OTf)$_2$. 740 μL of a 0.248 M CH_3CN solution of ligand **L3** (183.4 μmol) were added to 40.0 mg (91.7 μmol) of $Fe(OTf)_2(CH_3CN)_2$ under a N_2 atmosphere. The solution was stirred for 30 min, and the solvent was removed under reduced pressure. The dark purple solid was redissolved into anhydrous CH_2Cl_2 and filtered over Celite, and then crystals were obtained by slow diffusion of Et_2O (70 mg, 77% yield). X-ray quality crystals were grown by slow diffusion of diethyl ether into a dichloromethane solutions of $(\mathbf{L3})_2Fe(OTf)_2$. ^1H NMR (400 MHz, CD_3CN, 25 °C) δ 10.22 (s, 2H), 10.15 (s, 1.4 H), 8.20 (d, 2H, J = 8 Hz), 8.06 (s, 2H), 7.85 (m, 2H), 7.68 (m, 4H), 7.56 (d, 2H, J = 8 Hz), 7.49 (m, 2H), 7. 42 (m, 2H), 7.22 (m, 2H), 7.05 (m, 2H), 6.91 (d, 2H, J = 8 Hz), 6.59 (m, 8H), 2.40 (s, 6H), 2.29 (4.5 H). HRMS (ESI-TOF in CH_3CN) for $C_{27}H_{26}N_6O_3F_3SFe$: calcd, 627.1083 ($(\mathbf{L3})_2Fe(OTf)^+$); found, 627.1104. Elemental analysis for $C_{29}H_{28}Cl_2N_6O_6F_6S_2Fe$ ($(\mathbf{L3})_2Fe(OTf)_2{\cdot}CH_2Cl_2$): calcd: C, 40.43, H, 3.28, N, 9.76; found: C, 40.46, H, 3.62, N, 9.69. UV-vis: λ 358 nm (ε = 6100), λ 464 nm (ε = 3700), λ_{max} 557 nm (ε = 6400).

Complex (L4)$_2$Fe(OTf)$_2$. 615 μL of a 0.300 M CH_3CN solution of ligand **L4** (183 μmol) were added to 40.0 mg (91.7 μmol) of $Fe(OTf)_2(CH_3CN)_2$ under a N_2 atmosphere. The solution was stirred for 30 min, and the solvent was removed under reduced pressure. The dark purple solid was redissolved into anhydrous CH_2Cl_2 and filtered over Celite, and then crystals were obtained by slow diffusion of Et_2O (39 mg, 51% yield). Complex $(\mathbf{L4})_2Fe(OTf)_2$ can be prepared also by mixing $Fe(OTf)_2(CH_3CN)_2$ 4-nitro-2-formylpyridine and 2-picolylamine **1** in a 1:2:2 molar ratio in CH_3CN solution, as demonstrated by the UV-vis spectra (see pages SI 18 and SI 19 in the Supporting Information). ^1H NMR of this complex is too complex for an interpretation due to isomerization processes (*vide supra*). HRMS (ESI-TOF in MeOH) for $C_{24}H_{19}N_8O_4Fe$: calcd, 539.0879 ($(\mathbf{L4})_2Fe-H^+$); found, 539.0876. Elemental analysis for $C_{26}H_{20}N_8O_{10}F_6S_2Fe{\cdot}1.5CH_2Cl_2$ ($(\mathbf{L1})_2Fe(OTf)_2{\cdot}1.5CH_2Cl_2$): calcd: C, 34.197, H, 2.40, N, 11.60; found: C, 34.67, H, 2.64, N, 11.51. UV-vis: λ 418 nm (ε = 5000), λ 522 nm (ε = 5600), λ_{max} 618 nm (ε = 8600).

■ ASSOCIATED CONTENT

Supporting Information

The Supporting Information is available free of charge on the ACS Publications website at DOI: 10.1021/acs.inorgchem.5b01500.

NMR, ESI-TOF, UV-vis characterization of ligands and complexes, details of $(\mathbf{L1})_2Fe(OTf)_2$ and $(\mathbf{L3})_2Fe(OTf)_2$ X-ray characterization, UV–vis titrations, cyclic voltammetry of complex $(\mathbf{L1})_2Fe(OTf)_2$, preparation and oxidation procedures, oxidation results (PDF)

Crystallographic data for $C_{28}H_{26}F_6FeN_6O_6S_2$ (CIF)

Crystallographic data for $C_{25}H_{22}ClF_3FeN_6O_7S$ (CIF)

■ AUTHOR INFORMATION

Corresponding Authors

*E-mail: miquel.costas@udg.edu (M. Costas).

*E-mail: stefano.distefano@uniroma1.it (S. Di Stefano).

Author Contributions

All authors have given approval to the final version of the manuscript.

Funding

S.D.S. thanks the Italian Ministry of Education, University and Research (MIUR) (No. PRIN 2010CX2TLM). This work was also partially supported by Università di Roma La Sapienza-Area Supporto alla Ricerca (Progetti di Ricerca 2014 and Avvio alla Ricerca 2014). M.C. acknowledges financial support from ERC-2009-StG-239910 (to M.C.), the Spanish Ministry of Science (Nos. CTQ2012-37420-C02-01/BQU and CSD2010-00065, to M.C.) and Generalitat de Catalunya (ICREA Academia Award and No. SGR-862).

Notes

The authors declare no competing financial interest.

■ ACKNOWLEDGMENTS

The authors thank Mr. Simone Giosia and Mr. Stefano Aiello for their technical assistance in the preparation of complexes.

■ REFERENCES

(1) (a) Que, L., Jr.; Tolman, W. B. *Nature* **2008**, *455*, 333–340. (b) White, M. C. *Science* **2012**, *335*, 807–809. (c) Talsi, E. P.; Bryliakov, K. P. *Coord. Chem. Rev.* **2012**, *256*, 1418–1434.

DOI: 10.1021/acs.inorgchem.5b01500
Inorg. Chem. XXXX, XXX, XXX–XXX

(d) Company, A.; Lloret-Fillol, J.; Gómez, L.; Costas, M. In *Alkane C–H Activation by Single-Site Metal Catalysis*; Perez, P. J., Ed.; Springer: Dordrecht, The Netherlands, 2013; Vol. *38*.

(2) (a) Chen, M. S.; White, M. C. *Science* **2007**, *318*, 783–787. (b) Gómez, L.; Garcia-Bosch, I.; Company, A.; Benet-Buchholz, J.; Polo, A.; Sala, X.; Ribas, X.; Costas, M. *Angew. Chem., Int. Ed.* **2009**, *48*, 5720–5723. (c) Chen, M. S.; White, M. C. *Science* **2010**, *327*, 566–571. (d) Bigi, M. A.; Reed, S. A.; White, M. C. *J. Am. Chem. Soc.* **2012**, *134*, 9721–9726. (e) Hitomi, Y.; Arakawa, K.; Funabiki, T.; Kodera, M. *Angew. Chem., Int. Ed.* **2012**, *51*, 3448–3452. (f) Gómez, L.; Canta, M.; Font, D.; Prat, I.; Ribas, X.; Costas, M. *J. Org. Chem.* **2013**, *78*, 1421–1433. (g) Prat, I.; Gómez, L.; Canta, M.; Ribas, X.; Costas, M. *Chem.—Eur. J.* **2013**, *19*, 1908–1913. (h) Gormisky, P. E.; White, M. C. *J. Am. Chem. Soc.* **2013**, *135*, 14052–14055. (i) Clemente-Tejeda, D.; López-Moreno, A.; Bermejo, F. A. *Tetrahedron* **2013**, *69*, 2977–2986. (j) Nesterov, D. S.; Nesterova, O. V.; Guedes da Silva, M. F. C.; Pombeiro, A. J. L. *Catal. Sci. Technol.* **2015**, *5*, 1801–1812. (k) He, Y.; Gorden, J. D.; Goldsmith, C. R. *Inorg. Chem.* **2011**, *50*, 12651–12660. (l) Yazerski, V. A.; Spannring, P.; Gatineau, D.; Woerde, C. H. M.; Wieclawska, S. M.; Lutz, M.; Kleijn, H.; Klein Gebbink, R.R. J. M. *Org. Biomol. Chem.* **2014**, *12*, 2062–2017.

(3) (a) Oloo, W. N.; Fielding, A. J.; Que, L., Jr. *J. Am. Chem. Soc.* **2013**, *135*, 6438–6441. (b) Que, L., Jr. *Acc. Chem. Res.* **2007**, *40*, 493–500. (c) Nam, W. *Acc. Chem. Res.* **2007**, *40*, 522–531. (d) Bryliakov, K. P.; Talsi, E. P. *Coord. Chem. Rev.* **2014**, *276*, 73–96. (e) McDonald, A. R.; Que, L., Jr. *Coord. Chem. Rev.* **2013**, *257*, 414–428. (f) Ray, K.; Pfaff, F. F.; Wang, B.; Nam, W. *J. Am. Chem. Soc.* **2014**, *136*, 13942–13958.

(4) (a) Costas, M.; Chen, K.; Que, L., Jr. *Coord. Chem. Rev.* **2000**, *200–202*, 517–544. (b) Chen, K.; Que, L., Jr. *J. Am. Chem. Soc.* **2001**, *123*, 6327–6337. (c) Roelfes, G.; Lubben, M.; Hage, R.; Que, L., Jr.; Feringa, B. L. *Chem.—Eur. J.* **2000**, *6*, 2152–2159. (d) Thibon, A.; Jollet, V.; Ribal, C.; Senechal-David, K.; Billon, L.; Sorokin, A. B.; Banse, F. *Chem.—Eur. J.* **2012**, *18*, 2715–2724. (e) For an example that blocking of coordination sites leads to Fenton activation of H_2O_2, see: Mekmouche, Y.; Ménage, S.; Toia-Duboc, C.; Fontecave, M.; Galey, J.-B.; Lebrun, C.; Pecaut, J. *Angew. Chem., Int. Ed.* **2001**, *40*, 949–952. (f) MacFaul, P. a.; Ingold, K. U.; Wayner, D. D. M.; Que, L. *J. Am. Chem. Soc.* **1997**, *119*, 10594–10598. (g) Puri, M.; Que, L. *Acc. Chem. Res.* **2015**, *48*, 2443–2452. (h) Mairata i Payeras, A.; Ho, R. Y. N.; Fujita, M.; Que, L. *Chem.—Eur. J.* **2004**, *10*, 4944–4953. (i) Zhang, Q.; Goldsmith, C. R. *Inorg. Chem.* **2014**, *53*, 5206.

(5) (a) Mas-Ballestè, R.; Que, L., Jr. *J. Am. Chem. Soc.* **2007**, *129*, 15964–15972. (b) Wang, Y.; Janardanan, D.; Usharani, D.; Han, K.; Que, L., Jr.; Shaik, S. *ACS Catal.* **2013**, *3*, 1334–1341. (c) Oloo, W. N.; Meier, K. K.; Wang, Y.; Shaik, S.; Münck, E.; Que, L., Jr. *Nat. Commun.* **2014**, *5*, 3046–3054. (d) Oloo, W. N.; Que, L. *Acc. Chem. Res.* **2015**, *48*, 2612–2621.

(6) (a) Prat, I.; Company, A.; Postils, V.; Ribas, X.; Que, L., Jr.; Luis, J. M.; Costas, M. *Chem.—Eur. J.* **2013**, *19*, 6724–6738. (b) Prat, I.; Mathieson, J. S.; Güell, M.; Ribas, X.; Luis, J. M.; Cronin, L.; Costas, M. *Nat. Chem.* **2011**, *3*, 788–793. (c) Mitra, M.; Lloret-Fillol, J.; Haukka, M.; Costas, M.; Nordlander, E. *Chem. Commun.* **2014**, *50*, 1408–1410.

(7) (a) Bassan, A.; Blomberg, M. R. A.; Siegbahn, P. E. M.; Que, L., Jr. *J. Am. Chem. Soc.* **2002**, *124*, 11056–11063. (b) Lyakin, O. Y.; Bryliakov, K. P.; Britovsek, G. J. P.; Talsi, E. P. *J. Am. Chem. Soc.* **2009**, *131*, 10798–10799. (c) Yoon, J.; Wilson, S. A.; Jang, Y. K.; Seo, M. S.; Nehru, K.; Hedman, B.; Hodgson, K. O.; Bill, E.; Solomon, E. I.; Nam, W. *Angew. Chem., Int. Ed.* **2009**, *48*, 1257–1260.

(8) Hitomi, Y.; Arakawa, K.; Kodera, M. *Chem.—Eur. J.* **2013**, *19*, 14697–14701.

(9) Newhouse, T.; Baran, P. S. *Angew. Chem., Int. Ed.* **2011**, *50*, 3362–3374.

(10) (a) Ciaccia, M.; Cacciapaglia, R.; Mencarelli, P.; Mandolini, L.; Di Stefano, S. *Chem. Sci.* **2013**, *4*, 2253–2261. (b) Ciaccia, M.; Pilati, S.; Cacciapaglia, R.; Mandolini, L.; Di Stefano, S. *Org. Biomol. Chem.* **2014**, *12*, 3282–3287. (c) Ciaccia, M.; Di Stefano, S. *Org. Biomol. Chem.* **2015**, *13*, 646–654 and references therein cited..

(11) (a) Tang, J.; Gamez, P.; Reedijk, J. *Dalton Trans.* **2007**, 4644–4646. (b) Retcher, B.; Costa, J. S.; Tang, J.; Hage, R.; Gamez, P.; Reedijk, J. *J. Mol. Catal. A: Chem.* **2008**, *286*, 1–5. (c) Tanase, S.; Reedijk, J.; Hage, R.; Rothenberg, G. *Top. Catal.* **2010**, *53*, 1039–1044.

(12) (a) Lenze, M.; Martin, E. T.; Rath, N. P.; Bauer, E. B. *ChemPlusChem* **2013**, *78*, 101–116. (b) Shejwalkar, P.; Rath, N. P.; Bauer, E. B. *Dalton Trans.* **2011**, *40*, 7617–7631. (c) Britovsek, G. J. P.; England, J.; Spitzmesser, S. K.; White, A. J. P.; Williams, D. J. *Dalton Trans.* **2005**, 945–955. (d) Britovsek, G. J. P.; England, J.; White, A. J. P. *Dalton Trans.* **2006**, 1399–1408. (e) Martínez-Ferraté, O.; Britovsek, G. J. P.; Claver, C.; Van Leeuwen, P. W. N. M. *Inorg. Chim. Acta* **2015**, *431*, 156–160.

(13) Olivo, G.; Arancio, G.; Mandolini, L.; Lanzalunga, O.; Di Stefano, S. *Catal. Sci. Technol.* **2014**, *4*, 2900–2903.

(14) Codolà, Z.; Lloret-Fillol, J.; Costas, M. *Prog. Inorg. Chem.* **2014**, *59*, 447–531 and references cited therein..

(15) (a) Diebold, A.; Hagen, K. S. *Inorg. Chem.* **1998**, *37*, 215–223. (b) Blakesley, D. W.; Payne, S. C.; Hagen, K. S. *Inorg. Chem.* **2000**, *39*, 1979–1989. (c) Britovsek, G. J. P.; England, J.; White, A. J. P. *Inorg. Chem.* **2005**, *44*, 8125–8134. (d) Simaan, A. J.; Dopner, S.; Banse, F.; Bourcier, S.; Bouchoux, G.; Boussac, A.; Hildebrandt, P.; Girerd, J. J. *Eur. J. Inorg. Chem.* **2000**, *2000*, 1627–1633.

(16) (a) Holanda, M. I. D.; Krumholz, P.; Chum, H. L. *Inorg. Chem.* **1976**, *15*, 890–893. (b) Chavez-Gil, T. E.; Yasaka, M.; Senokuchi, T.; Sumimoto, M.; Kurosaki, H.; Goto, M. *Chem. Commun.* **2001**, 2388–2389.

(17) (a) Olivo, G.; Lanzalunga, O.; Mandolini, L.; Di Stefano, S. *J. Org. Chem.* **2013**, *78*, 11508–11512. (b) Cussó, O.; Garcia-Bosch, I.; Ribas, X.; Lloret-Fillol, J.; Costas, M. *J. Am. Chem. Soc.* **2013**, *135*, 14871–14878.

(18) Oloo, W. N.; Que, L. Jr. *Homogeneous Catalytic Applications*; Reedijk, J., Poeppelmeier, K., Eds; Comprehensive Inorganic Chemistry II: From Elements to Applications, Vol. *6*, 2nd Edition; Elsevier: Amsterdam, 2013; pp 763–778.10.1016/B978-0-08-097774-4.00627-6

(19) Russell, G. *J. Am. Chem. Soc.* **1957**, *79*, 3871–3877.

(20) The A/K ratio is 11.4 if all of the hydrogen peroxide is added at once. However, in preparative reactions, the yield is slightly decreased if all the H_2O_2 is added at once, probably because of the competing disproportionation reaction.

(21) (a) Trotman-Dickenson, A. F. *Adv. Free Radical Chem.* **1965**, *1*, 1–38. (b) Buxton, G. V.; Greenstock, C. L.; Helman, W. P.; Ross, A. B. *J. Phys. Chem. Ref. Data* **1988**, *17*, 513–886. (c) Simmons, E. M.; Hartwig, J. F. *Angew. Chem., Int. Ed.* **2012**, *51*, 3066–3072.

(22) (a) Costas, M.; Que, L., Jr. *Angew. Chem., Int. Ed.* **2002**, *41*, 2179–2181. (b) England, J.; Britovsek, G. J. P.; Rabadia, N.; White, A. J. P. *Inorg. Chem.* **2007**, *46*, 3752–3767. (c) Company, A.; Gómez, L.; Fontrodona, X.; Ribas, X.; Costas, M. *Chem.—Eur. J.* **2008**, *14*, 5727–5731.

(23) Meunier, B.; Robert, A.; Pratviel, G.; Bernadou, J. Metalloporphyrins in Catalytic Oxidation and Oxidative DNA Cleavage. In *The Porphyrin Handbook*; Kadish, K. M., Smith, K. M., Guilard. R., Eds.; Academic Press: New York, 2000.

(24) An excess of triphenylphosphine added to the final reaction mixture reduces the hydroperoxide eventually formed. If GC analysis of the reaction mixture does not significantly change before and after the addition of triphenyl phosphine, it can be concluded that hydroperoxide is not formed to a significant extent. See: Shulpin, G. B.; Nizova, G. V. *React. Kinet. Catal. Lett.* **1992**, *48*, 333–338.

(25) $H_2{}^{18}O$ incorporation is dependent on the H_2O concentration. However, saturation is usually reached before 1000 equiv of water (see ref 6).

(26) Such a lack of effect of acetic acid has been documented only once for a nonheme iron complex bearing a pentadentate ligand. In this case, Hitomi et al.[2e] rationalized that the powerful electron-donating ability of an amide moiety binding to the ferric center *trans* to the hydroperoxide ligand exerted a push-effect that facilitated heterolytic O–O cleavage.

DOI: 10.1021/acs.inorgchem.5b01500
Inorg. Chem. XXXX, XXX, XXX–XXX

(27) Chen, K.; Costas, M.; Kim, J.; Tipton, A. K.; Que, L., Jr. *J. Am. Chem. Soc.* **2002**, *124*, 3026.
(28) Complex $(terpy)_2{\cdot}Fe(OTf)_2$ was obtained as described in: Braterman, P. S.; Song, J.-I.; Peacock, R. D. *Inorg. Chem.* **1992**, *31*, 555−559.
(29) Condensation of amine **2** with 2-picolylaldehyde to give imine **1.5** was found to be much slower than condensation of amine **1** with 2-picolylaldehyde to give imine **1.1**, the former being complete within 20 h, and the latter being complete within 40 min.
(30) Rowland, J. M.; Olmstead, M. M.; Mascharak, P. K. *Inorg. Chem.* **2002**, *41*, 2754−2760.
(31) (a) Barton, D. H. R.; Doller, D. *Acc. Chem. Res.* **1992**, *25*, 504. (b) Kiani, S.; Tapper, A.; Staples, R. J.; Stavropoulos, P. *J. Am. Chem. Soc.* **2000**, *122*, 7503−7517.
(32) Such an induction period is more difficult to be noticed under cyclohexane oxidation conditions, probably because of the ∼10-fold increase in reagents concentration and the corresponding enhancement in reaction rates.
(33) (a) Comba, P.; Rajaraman, G. *Inorg. Chem.* **2008**, *47*, 78−93. (b) Bukowski, M. R.; Comba, P.; Lienke, A.; Limberg, C.; Lopez de Laorden, C.; Mas-Ballesté, R.; Merz, M.; Que, L., Jr. *Angew. Chem., Int. Ed.* **2006**, *45*, 3446−3449. (c) Oldenburg, P. D.; Feng, Y.; Pryjomska-Ray, I.; Ness, D.; Que, L., Jr. *J. Am. Chem. Soc.* **2010**, *132*, 17713−17723.
(34) Juris, A.; Balzani, V.; Barigelletti, F.; Campagna, S.; Belser, P.; Von Zelewsky, A. *Coord. Chem. Rev.* **1988**, *84*, 85−278.
(35) Taktak, S.; Ye, W.; Herrera, A. M.; Rybak-Akimova, E. V. *Inorg. Chem.* **2007**, *46*, 2929−2942.
(36) Wang, D.; Ray, K.; Collins, M. J.; Farquhar, E. R.; Frisch, J. R.; Gómez, L.; Jackson, T. A.; Kerscher, M.; Waleska, A.; Comba, P.; Costas, M.; Que, L., Jr. *Chem. Sci.* **2013**, *4*, 282−291 and references therein.
(37) Ortiz De Montellano, P. R. *Chem. Rev.* **2010**, *110*, 932−948.
(38) For an example of an oxoiron(IV) complex supported by an iminopyridine ligand, see: Badiei, Y. M.; Siegler, M. A.; Goldberg, D. P. *J. Am. Chem. Soc.* **2011**, *133*, 1274−1277.
(39) Hagen, K. S. *Inorg. Chem.* **2000**, *39*, 5867−5869.
(40) Comba, P.; Morgen, M.; Wadepohl, H. *Inorg. Chem.* **2013**, *52*, 6481−6501.

DOI: 10.1021/acs.inorgchem.5b01500
Inorg. Chem. XXXX, XXX, XXX−XXX